Geophysical Research Letters

RESEARCH LETTER
10.1029/2019GL084495

Special Section:
Carbon and Weather: Results from the Atmospheric Carbon and Transport – America Mission

Forward Modeling and Optimization of Methane Emissions in the South Central United States Using Aircraft Transects Across Frontal Boundaries

Z. R. Barkley[1], K. J. Davis[1], S. Feng[1], N. Balashov[2,3], A. Fried[4], J. DiGangi[5], Y. Choi[5], and H. S. Halliday[5]

[1]Department of Meteorology and Atmospheric Science, The Pennsylvania State University, University Park, PA, USA, [2]Global Modeling and Assimilation Office, NASA Goddard Space Flight Center, Greenbelt, MD, USA, [3]Universities Space Research Association, Columbia, MD, USA, [4]Institute of Arctic and Alpine Research, University of Colorado Boulder, Boulder, CO, USA, [5]Langley Research Center, National Aeronautics and Space Administration, Hampton, VA, USA

Key Points:
- Methane and ethane observations from U.S. Midwest frontal flights are used to solve for emissions from oil/gas and animal agriculture
- Methane emissions from oil/gas sectors in the South Central United States are 1.8 ± 0.7 (2σ) times larger than U.S. EPA inventory estimates
- Measurements across frontal structures can provide opportunities to solve for regional emissions of trace gases in other regions

Supporting Information:
- Supporting Information S1

Correspondence to:
Z. Barkley,
zrb5027@psu.edu

Citation:
Barkley, Z. R., Davis, K. J., Feng, S., Balashov, N., Fried, A., DiGangi, J., et al. (2019). Forward modeling and optimization of methane emissions in the South Central United States using aircraft transects across frontal boundaries. *Geophysical Research Letters*, *46*, 13,564–13,573. https://doi.org/10.1029/2019GL084495

Received 12 JUL 2019
Accepted 21 OCT 2019
Accepted article online 29 OCT 2019
Published online 26 NOV 2019
Corrected 11 MAY 2020

This article was corrected on 11 MAY 2020. See the end of the full text for details.

Abstract The South Central United States is a hot spot for anthropogenic methane (CH_4) emissions, with contributions from the oil/gas (O&G) and animal agriculture sectors. During frontal weather events, airflow combines enhancements from these emissions into a large plume. In this study, we take CH_4 and ethane (C_2H_6) observations from the Atmospheric Carbon and Transport-America campaign and adjust O&G and animal agriculture emissions such that modeled CH_4 and C_2H_6 enhancements match the observed plume. Results from the joint CH_4-C_2H_6 optimization indicate that emissions from the O&G sector are 1.8 ± 0.7 (2σ) times larger than EPA inventory estimates. These results match synthesis work from recent literature and reject the possibility that this increase compared to inventories is due to a potential bias in daytime-only measurements of these facilities. Successful modeling from this study raises the possibility of using trace gas measurements along frontal crossings to solve for emissions in other regions of the United States.

1. Introduction

Methane (CH_4) is a potent greenhouse gas with 28–35 times the warming potential of carbon dioxide (CO_2) over a 100 year period. Increases in global CH_4 concentrations since the preindustrial era have contributed approximately 20% to the increased radiative forcing on the planet (Myhre et al., 2013). According to the U.S. Environmental Protection Agency (EPA), the two largest sources of anthropogenic CH_4 emissions in the Unite States originate from oil and natural gas (O&G) production and animal agriculture. Together these sources contributed 18 Tg CH_4 in the year 2016, or 67% of anthropogenic CH_4 emissions in the United States (US Environmental Protection Agency, 2018). However, large uncertainties exist regarding the accuracy of these assessments.

CH_4 emissions from O&G infrastructure are a complex source to quantify. Numerous opportunities exist for CH_4 to escape into the atmosphere through both planned and unplanned releases in the O&G supply chain, from the drilling and production of the wells (Allen et al., 2013), to the gathering and processing facilities (Mitchell et al., 2015), to the transmission and storage of the gas (Zimmerle et al., 2015), and finally, the distribution for end use (McKain et al., 2015; Balashov et al., 2019). To document and quantify these emissions, the EPA primarily relies on a bottom-up methodology, collecting component and device-level counts and multiplying them by an average emission rate based on values found in scientific literature (US Environmental Protection Agency, 2019). Independent top-down measurements of O&G basins in the last decade have found varying CH_4 emission rates across basins (Peischl et al., 2016, Peischl et al., 2018), but almost always with a total emission rate higher than EPA-derived bottom-up estimates (Brandt et al., 2014; Barkley et al., 2019). Synthesis work accounting for various independent site-level measurements of wellpads and facilities estimate that EPA emission estimates from the O&G production sector are low by a factor of 1.5 or more (Alvarez et al., 2018; Omara et al., 2018). The discrepancy between these inventory estimates is thought to be caused by an underattribution of emissions related to abnormal operating conditions, sources with less predictable spatial and temporal variability that may be difficult to capture in a bottom-up inventory

(Zavala-Araiza et al., 2015). Because CH_4 emissions from the production sector are the largest source of emissions from O&G operations, uncertainty from these sources dominate the overall uncertainty of emissions from O&G operations. (US Environmental Protection Agency, 2019; Alvarez et al., 2018).

Similar issues have arisen concerning CH_4 emissions from the animal agriculture sector. CH_4 emissions from animal agriculture come from two primary sources: emissions from enteric fermentation in ruminants and emissions through manure management. Through the use of emission factors and inventory counts, the EPA provides annual estimates of CH_4 emissions from enteric fermentation and manure management (US Environmental Protection Agency, 2019). This bottom-up inventory estimate matches total emission estimates from two independent bottom-up assessments, though spatial discrepancies exist between them (Hristov et al., 2017; EDGAR, 2011). However, top-down estimates performed on the scale of individual farms (Desjardins et al., 2018), states (Cui et al., 2017), and continents (Miller et al., 2013) have attributed higher CH_4 emissions to animal agriculture compared to their bottom-up counterparts.

One of the largest regions of CH_4 emissions in the United States from both O&G and animal agriculture can be found in the South Central Unites States. The objective of this study is to independently quantify emissions from these sectors in the South Central United States through a top-down approach. Observations from frontal transects downwind of the region are combined with forward modeling techniques to quantify CH_4 emissions from the O&G and animal agriculture sector and compare them directly with the EPA 2012 Gridded CH_4 inventory (Maasakkers et al., 2016). Continuous ethane (C_2H_6) observations are used to separate out and solve for CH_4 emissions specifically from O&G sector.

2. Methods

2.1. Observations and Study Region

Observations from this study come from aircraft measurements obtained in the Atmospheric Carbon and Transport-America (ACT-America) campaign. Airborne CH_4 from the ACT-America flights was measured using a commercial PICARRO G2401-m instrument adapted with a custom inlet system for drying and conditioning the sample air (DiGangi et al., 2018). Calibrations were performed hourly in-flight using standards obtained from NOAA ESRL and traceable to the WMO X2004A scale (Dlugokencky et al., 2005). Continuous C_2H_6 measurements were acquired from the CAMS-2 (Compact Airborne Multi-Species Spectrometer) instrument designed and operated by the University of Colorado (Barkley et al., 2019). Continuous measurements for both CH_4 and C_2H_6 were averaged over 5 min time intervals to reduce structural noise created by more local sources. For two flights (2 November 2017 and 18 October 2017 northern transect), continuous C_2H_6 data from the CAMS-2 were not available. For these flights, multispecies flask samples with a temporal frequency of approximately 20 min were used to quantify C_2H_6 concentrations (Sweeney et al., 2015).

The focus of this study was to quantify CH_4 emissions from the south central region of the United States (27–42°N 90–105°W; see Figure 1). Spatially, a large percentage of United States CH_4 emissions are concentrated in this region, primarily due to presence of both O&G production as well as animal agriculture (Maasakkers et al., 2016). Major O&G basins can be found in this area, such as the Anadarko, Eagle Ford, Fayetteville, Haynesville, Permian, and Barnett. When added together, these basins account for 40% of O&G produced in the United States in 2017 (US Energy Information Administration, 2018). In addition, this region also contains 25% of cattle raised in the country (USDA, 2014). The combination of these sources makes the entire South Central United States a hot spot for CH_4 emissions.

Observations in the atmospheric boundary layer (ABL) from five ACT flights were used in this study that specifically target emissions from the South Central United States, four of which took place in fall of 2017 and one of which occurred in February of 2017 (Figure S2). The flight on 18 October 2017 was separated into two transects (south and north) during analysis, resulting in six total transects. A potential seventh frontal transect occurring on 30 October 2017 was not used in the analysis due to a failure to accurately model the meteorology on that day (see supporting information section S3). Flights that crossed frontal systems were specifically selected for this experiment. These flights share certain characteristics that make them useful for emissions quantification; persistent southerly steady-state winds east of a frontal system transport air quickly across the various sources in the South Central United States and converge along the frontal boundary, combining their enhancements into an identifiable plume, which can be observed in all transects (see supporting information section S1). Furthermore, the distinct features of frontal systems along the boundaries (i.e., wind shifts and temperature changes) make it easier to characterize differences between

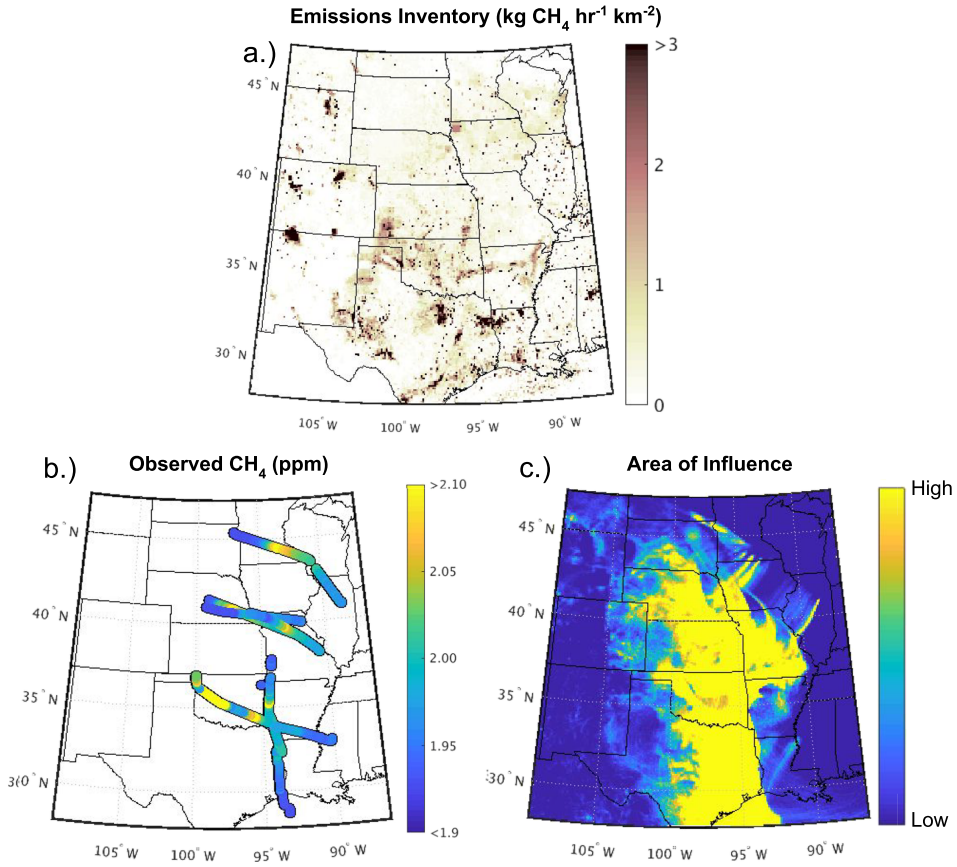

Figure 1. (a) Total CH_4 emissions (kg hr^{-1} kg^{-2}) from the 2012 EPA Gridded Inventory for the month of October. (b) Boundary layer CH_4 observations (ppm) from the six transects used in this study. (c) Summed influence functions from the six transects showing the surface areas that had the most influence on the measurements.

the observed versus the modeled transport of the plumes and quantify errors in the atmospheric transport reanalysis.

2.2. Model and Emissions Inventory

To model CH_4 enhancements for the six transects, the Weather Research and Forecasting model was used with chemistry enabled. A 9 km resolution domain was created encompassing the South Central and Midwestern United States, with multiple chemically-inert tracers used to track different sources of CH_4. The Weather Research and Forecasting configuration for the model physics used in this research includes the use of the double-moment scheme for cloud microphysical processes, the rapid radiative transfer method for general circulation models, the Level 2.5 turbulence kinetic energy -predicting Mellor–Yamada–Nakanishi–Niino (MYNN) planetary boundary layer scheme, and the Noah 4-layer land-surface model. Additionally, three different reanalysis products were used as initialization and driver data to create three separate model runs for each flight: the North American Regional Reanalysis model, the Global Forecasting System, and the ERA-I reanalysis product (Mesinger et al., 2006; Dee et al., 2011). These differing runs were used as a method to assess potential transport errors for each flight (Díaz-Isaac et al., 2018).

Anthropogenic CH_4 emissions used as input for the model come from the Gridded 2012 Methane Emissions Inventory (Maasakkers et al., 2016). Separate tracers were used for emissions from the O&G sector, enteric fermentation, and manure management (animal agriculture), and an additional tracer for all other small sources. The O&G sector was broken down further into tracers roughly outlining the Anadarko, Woodford, Permian, Fort Worth, East Texas, and Gulf. Potential emissions from sources in northern Mexico were insignificant compared to emissions within the South Central United States and are not included in the model inventory (Sheng et al., 2017; EDGAR, 2011). For wetland emissions, the mean ensemble value of

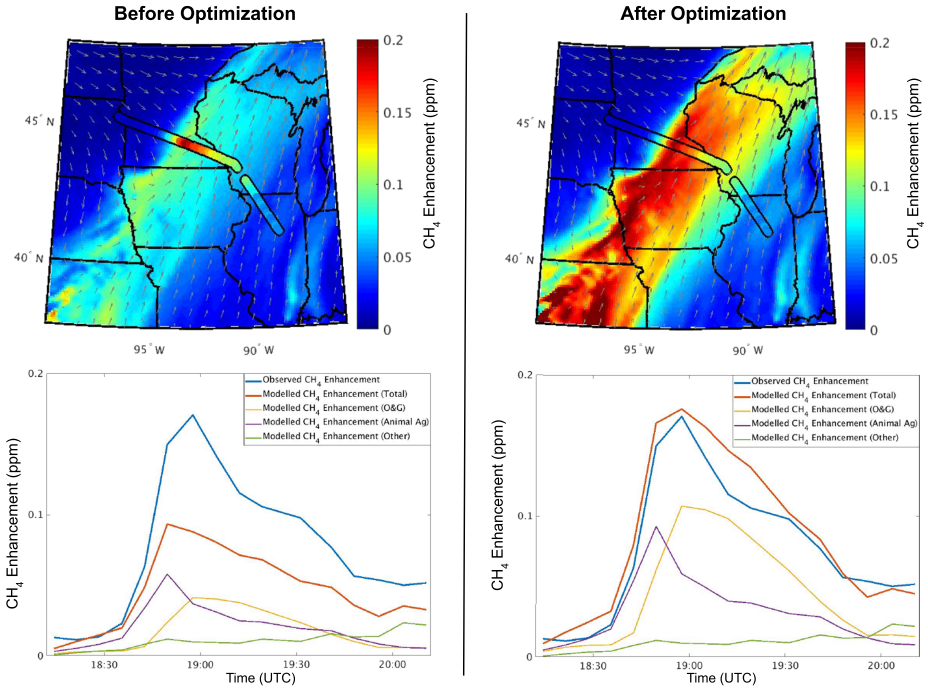

Figure 2. (top left) Observed vs. modeled CH_4 for the northern transect of the flight on 18 October 2017 using the unadjusted emissions from the EPA Gridded Methane Inventory. (bottom left) Time series of observed (blue) versus modeled (red) CH_4 enhancements along the flight track, with a breakdown of the O&G, animal agriculture, and other modeled CH_4 enhancements contributing to the total model enhancement. (right) Same as left, but after optimizing emissions from O&G and animal agriculture.

WetCHARTs v1.0 was used to show that wetland sources had minimal mole fraction on flights used in this study but was not utilized in the final solution due to limited data on their emissions (Bloom et al., 2017). Only one flight (21 October 2017) had a modeled wetlands plume intersecting the transect, but the spatial pattern of the enhancement did not coincide with enhancements from the main O&G and animal agriculture plume and observations did not indicate an enhancement within the wetlands CH_4 plume. In addition to a CH_4 emissions inventory, a simplified C_2H_6 inventory is created for the region by multiplying CH_4 emissions from different basins with their respective C_2H_6:CH_4 ratios (TCEQ, 2012; Ellis, 2014) (see supporting information section S2 for details).

2.3. Methane Optimization Technique

For each flight, the objective is to scale CH_4 emissions for O&G and animal agriculture sources within the model by a linear coefficient to find optimized emission rates that closest match the observed plumes (Figure 2). This is done through minimizing the squared error as shown in the following equation:

$$J^{CH_4} = \sqrt{\sum_{i=1}^{n} (X_i^{CH_4} - Y_i^{CH_4})^2} \tag{1}$$

where X_i is the observed CH_4, Y_i is the modeled CH_4 at each observation, and J is a cost function we are trying to minimize. Whereas X_i is only the aircraft-observed CH_4 along the transect, the model CH_4 Y_i is composed of multiple terms, given in the equation below

$$Y_i^{CH_4} = C_1 Y_i^{OG} + C_2 Y_i^{agriculture} + Y_i^{Other} + B^{CH_4} \tag{2}$$

where the total modeled CH_4 $Y_i^{CH_4}$ is composed of four terms. Y^{OG} and $Y^{agriculture}$ are the modeled O&G and animal agriculture enhancements and are both preceded by a constant C_1 and C_2 to allow their concentrations to vary linearly in the optimization. Because modeled concentrations adjust linearly with their emissions, the C_1 and C_2 values that minimize equation (1) represent emission rate multipliers for each sector that optimize the match between the observations and the model. Y^{Other} is the modeled enhancement

from the remaining sources and is not solved for in the optimization approach. B^{CH_4} is a background value applied to the modeled enhancement that accounts for CH_4 concentrations specific to the air mass that originate from outside the model domain. Because frontal flights contain observations in two different air masses, a background B^{CH_4} must be applied to data points specific to each air mass. We determine the location of the change in air mass by a sharp transition in potential temperature, dew point, and wind direction, and then calculate B^{CH_4} for each air mass. To calculate B^{CH_4}, we first find the CH_4 mole fraction from the lowest 10th percentile of observations in the ABL from that air mass. This value typically comes from the edge of a transect away from the major regional CH_4 plume and is closest to representing the background value of the regional air mass. After selecting this observed background concentration we then select the modeled background concentration, found by choosing the lowest 10th percentile of modeled enhancements along the flight path within the same air mass. By taking the difference between the observed background and modeled background concentrations, we create a background value B^{CH_4} that can be added to the modeled enhancements to align the low points in the observations with the low points in the model. This can be represented through the following equation:

$$B^{CH_4} = X_{10\%}^{CH_4} - Y_{10\%}^{CH_4} \tag{3}$$

where $X_{10\%}$ and $Y_{10\%}$ are the 10th percentile of observations and modeled enhancements in a given air mass. Because the chosen background value is partially dependent on modeled enhancements, different C_1 and C_2 values in the model optimization will produce different $Y_{10\%}$ (and, thus, a different B). Because regional sources dominate over chemistry sinks at the surface for CH_4, a lower limit can be placed on the background value equal to CH_4 values observed in the free troposphere during each flight. Any B^{CH_4} that drops below this limit is set equal to it.

2.4. Ethane and Joint Optimization

In addition to CH_4 observations, C_2H_6 observations were also available from the six transects, four in the form of continuous measurements and the remaining two in lower frequency flask measurements across the transect. In order to model C_2H_6 concentrations, CH_4 emissions from the different O&G basins in the South Central United States were converted to C_2H_6 emissions using measured C_2H_6:CH_4 ratios from each basin (see supporting information section S2). C_2H_6 emissions from smaller sources, such as biomass burning, were not considered due to the much smaller magnitude of emissions from these sources. Similar to CH_4, the squared error was minimized to solve for the optimized emission rates

$$J^{C_2H_6} = \sqrt{\sum_{i=1}^{n} (X_i^{C_2H_6} - Y_i^{C_2H_6})^2} \tag{4}$$

where $J^{C_2H_6}$ is the squared error between the observed C_2H_6 $X_i^{C_2H_6}$ and modeled C_2H_6 $Y_i^{C_2H_6}$. With the O&G sector being the only significant source of C_2H_6, $Y_i^{C_2H_6}$ is calculated from the equation

$$Y_i^{C_2H_6} = C_1 Y_i^{OGC_2H_6} + B^{C_2H_6} \tag{5}$$

where $Y_i^{OGC_2H_6}$ is the modeled C_2H_6 enhancements from O&G sources, C_1 is the same multiplier from equation (2) used to find the optimized values between the observed and modeled C_2H_6, and $B^{C_2H_6}$ is a constant background value applied to the modeled enhancements. $B^{C_2H_6}$ is computed similarly to B^{CH_4} in equation (3), with the lower limit for $B^{C_2H_6}$ set to 0.

A final emissions optimization was performed to simultaneously optimize CH_4 and C_2H_6 emissions for each transect. For this optimization, O&G and animal agriculture emissions were adjusted to minimize the sum of the cost functions in equations (1) and (4).

$$J^{Joint} = \frac{J^{CH_4}}{iqr(\vec{X}^{CH_4})} + \frac{J^{C_2H_6}}{iqr(\vec{X}^{C_2H_6})} \tag{6}$$

where J^{Joint} is the sum of both the CH_4 and C_2H_6 cost functions normalized by the interquartile range of their respective observations. By normalizing each cost function by the interquartile range of their observations, each cost function is given a near-equal weighting in its contribution toward the joint cost function.

2.5. Uncertainty Analysis

Throughout the optimization, four categories of uncertainty exist that can influence the final result: uncertainty in the simulated atmospheric transport, uncertainty in the background value, uncertainty in the nonoptimized emissions, and uncertainty in the C_2H_6:CH_4 ratios of the O&G basins (used in the C_2H_6 optimization). To quantify these uncertainties, a Monte Carlo is used to draw random variables for each category and apply them in the optimization formula. For atmospheric transport errors, at the start of the optimization process one of the three transport models runs is randomly drawn and its enhancements are used, creating variability in the plume structures. To account for uncertainty in the background value, the value is first selected based on the observations and then a normal random variable with $\mu = 0$ and $\sigma = \pm 5$ ppb is added to the chosen background. Uncertainty in the unsolved emissions comes mostly from landfills and is represented by scaling enhancements from Y^{Other} by a normal random multiplier with $\mu = 1$ and $\sigma = \pm 0.25$. Finally, for uncertainty in the assumed C_2H_6:CH_4 ratio of each O&G basin, a normal random variable is drawn with $\mu = 0$ and $\sigma = \pm 0.03$ for each basin and applied to their ratio. This process is performed 1,000 times for each flight, and the spread produced in the optimized O&G and animal agriculture solutions is used to represent the uncertainty range. For more information on each source of uncertainty, the values chosen to represent them, and their impacts on the overall solution, refer to section S4 in the supporting information section.

A final source of uncertainty exists related to errors in the modeled wind speed and plume mixing depth. These errors can impact the magnitude of the modeled enhancement within the ABL, with high/low biases in modeled winds and mixing height resulting in a diluted/increased modeled tracer enhancement inside the ABL. To correct these biases, the following equation is applied (Barkley et al., 2017) to the modeled enhancements:

$$Y_{adj} = Y * \frac{U_m * z_m}{U_{obs} * z_{obs}} \tag{7}$$

where Y_{adj} is the corrected model enhancement calculated for each flight, Y is the original modeled enhancement, $\frac{U_m}{U_{obs}}$ is the mean modeled wind speed divided by the mean observed wind speed along the transect, and $\frac{z_m}{z_{obs}}$ is the mean modeled ABL depth divided by the observed ABL depth along the transect. To calculate the ABL depth, observations from aircraft vertical spirals performed along each transect are compared to the model data at the same location to find the height where CO_2, CH_4, and H^2O values experience a significant change to free tropospheric values and a sharp increase in potential temperature is observed (see supporting information section S3 for model performance).

The Eulerian-based methodology to scale emissions using a forward modeling approach is dependent on having a reliable spatial mapping of the locations of CH_4 emitters. The EPA gridded CH_4 emissions inventory used as the prior in this study is based on county-level or higher resolution data containing the locations of all anthropogenic sources of CH_4 in the United States. Though the magnitude of emissions from sources within this prior can potentially be flawed, the location of sources is well documented, reducing the likelihood of potential errors in the optimization from poor spatial mapping of the emissions. However, if major sources of CH_4 are missing or misplaced within the inventory, it would present errors that are not accounted for in the uncertainty assessment performed in this study.

3. Results and Discussion

Through the adjustment of O&G and animal agriculture emissions with a linear multiplier, modeled results of frontal flights are able to match observations from the ACT-America campaign to a high degree of accuracy (see Figure S5). The mean Pearson correlation coefficient for the six transects used in this study is 0.94, providing confidence in the ability of the model to reconstruct the location of the major CH_4 plume. Despite this accuracy, correctly desegregating and attributing the observed CH_4 to either the O&G or animal agriculture sector is difficult when only using CH_4 data. The mean optimized O&G and animal agriculture emissions across all flights center around 1.3 times their EPA inventory estimates, indicating that the EPA's total CH_4 inventory estimate for the South Central United States is too low. However, the potential range of solutions for each source individually is broad, with mean and 2σ confidence intervals of $1.5x \pm 0.7$ and $1.3x \pm 0.9$ for O&G and animal agriculture respectively (Figure 3). Part of the reason for the large variances on these sources is the colinearity of the optimized animal agriculture and O&G emission solutions. In many cases, similar matches between the model and the observations can be achieved by lowering emissions from

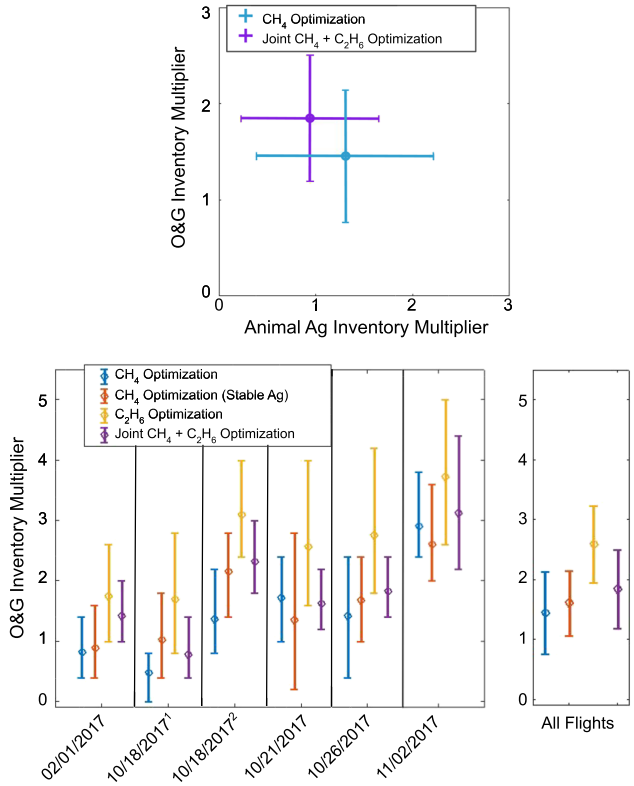

Figure 3. (top) Mean and 95% confidence intervals of the optimized emission rate multipliers for O&G and animal agriculture using the CH_4 optimization and the $CH_4 + C_2H_6$ joint optimization. (bottom) Flight by flight mean and 95% confidence intervals of the optimized emissions for O&G using various optimization strategies. (blue) Both O&G and animal agriculture inventories were optimized using CH_4 data. (red) Only O&G inventories were optimized using CH_4, keeping animal agriculture values constrained by their inventory data. (yellow) O&G inventories were optimized using only C_2H_6 data. (purple) Both O&G and animal agriculture inventories were optimized using the joint $CH_4 + C_2H_6$ technique.

one sector and raising the other equivalently. This colinearity is a consequence of using frontal flights to solve for emissions, as transport from these systems leads to the development of a single, well-defined plume along the boundary mixing together enhancements from all sources along its path.

Results from the C_2H_6 optimization can be used as a separate means to solve for O&G emissions and identify which source is responsible for the increased total CH_4 emissions observed from the CH_4 optimization. Similar to the CH_4 optimization, modeled C_2H_6 enhancements matched closely with observations, with a mean correlation coefficient of 0.82 for the six transects using the optimized solutions (Figure S6). From the results of the C_2H_6 optimization, total emissions from O&G are $2.6x \pm 0.6$ larger than EPA inventory estimates. These values are on the high end/exceed the uncertainty range for O&G from the CH_4 optimization and indicate that the overall increase in CH_4 emissions observed compared to EPA inventory estimates are likely associated with O&G sources and not animal agriculture. The joint CH_4-C_2H_6 optimization provides further evidence, producing mean and 2σ confidence intervals for O&G and animal agriculture emission multipliers of $1.8x \pm 0.7$ and $0.9x \pm 0.7$ respectively (Figure 3).

A different optimization was performed to provide an additional check on O&G emissions rates using the CH_4 data, but treating animal agriculture as a potential source of uncertainty in the Monte Carlo rather than an unbounded parameter to be solved for in the optimization. In this experiment, animal agriculture is set to have an emission rate and uncertainty range equal to the values in the EPA's gridded inventory estimate ($\sigma = \pm 7.5\%$) and is a variable drawn randomly from the Monte Carlo, with O&G emissions being the only variable optimized. The results of this test represent a solution range for O&G emissions that would be representative of the truth if one had high confidence in the EPA's animal agriculture estimates. From

this optimization, we find a mean and 2σ confidence interval for the O&G emission multiplier to be $1.6x \pm 0.5$. The close match between the results from this test and the CH_4-C_2H_6 joint optimization provides more confidence that the higher values of CH_4 observed from these flights can likely be attributed to the O&G sector.

From these various optimization methods, one major discrepancy that arises is the difference between the O&G emission rate solution when optimized using only CH_4 ($1.5\pm$ 0.7 from two-source optimization or $1.6x \pm 0.5$ for O&G only optimization) versus optimizing using only the C_2H_6 data ($2.6x \pm 0.6$). The difference between these two solutions is likely due to either a missing source of C_2H_6 in the simplified C_2H_6 inventory or a underestimation of the C_2H_6:CH_4 ratios assumed in this study to create the C_2H_6 inventory. To explore the latter scenario, a simplified C_2H_6 optimization was rerun, applying the same C_2H_6:CH_4 ratio to all basins uniformly and adjusting this ratio to observe its impact on the optimized O&G emission rate (see supporting information section S4). From this experiment, we find that applying a flat C_2H_6:CH_4 ratio of 0.13 produces solutions for O&G emissions using the C_2H_6 optimization that are nearly identical to the solutions from the CH_4 optimization both overall and flight-by-flight, with an absolute mean difference between the O&G rates per flight from these two solutions of only 0.15. The strong correlation between the results of these two optimizations after increasing the C_2H_6:CH_4 ratio by 80% of its original value (0.13 vs 0.07) indicates that C_2H_6:CH_4 emission ratios used in the simplified C_2H_6 inventory may be significantly lower than the true ratios, and could be related to an underestimation of emissions from oil-producing sectors of basins with a much lower percentage of CH_4 content (Gherabati et al., 2016; Cardoso-Saldaña et al., 2019).

From the CH_4-C_2H_6 joint optimization, we estimate O&G emissions from the South Central United States to be $1.8x \pm 0.7$ higher than 2012 EPA inventory estimates. This result is in agreement with national-scale aggregated estimates derived in Alvarez et al. (2018) (1.5–1.9x) and Omara et al. (2018) (1.5-3.3x, production sector only), as well as numerous top-down estimates of individual basins which have measured emissions higher than inventory estimates (Brandt et al., 2014). For top-down studies, there have been concerns that these estimates may contain bias due to their reliance of daytime measurements, unable to account for potential diurnal differences in O&G emissions that could exist due to different levels of onsite maintenance and activity (Vaughn et al., 2018). The flights from this study provide evidence to the contrary. For each flight, air traveled multiple days and nights across O&G basins before being measured by the aircraft. Their measurements represent emissions that are not only a mixture of the various basins in the South Central United States but are also mixture of daytime and nighttime emissions in the region (Figure S3). For this reason and given the large amount of O&G activity captured in these frontal plumes, it is unlikely that diurnal differences in O&G emission rates could explain the high emission rates observed in this study.

4. Conclusion

Using CH_4 and C_2H_6 observations from six aircraft transects crossing frontal systems in the South Central and Midwestern United States, we conclude that regional CH_4 emissions from the O&G sector are 1.8 ± 0.7 times higher than the 2012 EPA Gridded inventory (2σ confidence). Projected emissions from animal agriculture do not show significant differences from EPA inventory estimates ($0.9x \pm 0.7$), and large C_2H_6 mole fractions within the observed frontal plumes indicate increases in CH_4 emissions relative to inventory estimates are due to emissions from the O&G sector. Optimizing for O&G emissions using CH_4 and C_2H_6 observations individually results in inventory multipliers of 1.6 ± 0.5 using CH_4 and 2.6 ± 0.6 using C_2H_6. Discrepancies between the two solutions is likely due to an underestimation of the C_2H_6:CH_4 ratios assumed to represent the O&G basins in the study.

This study demonstrates the potential of using frontal systems to quantify CH_4 emissions from regional hot spots that span thousands of kilometers. The continuous, strong steady-state winds in the warm sector combined with the buildup of CH_4 along the frontal boundary can lead to the development of large plumes that represent enhancements from a large portion of O&G and animal agriculture emissions and are easily tracked within the model. Using this targeted approach to emissions quantification based on frontal weather patterns can serve as an alternative approach to quantifying fluxes on a regional scale. Future studies examining the strengths and weaknesses of emission quantification under different synoptic-scale weather patterns could provide valuable information for flight design.

Acknowledgments
The Atmospheric Carbon and Transport (ACT)-America project is a NASA Earth Venture Suborbital 2 project funded by NASAâ's Earth Science Division (Grant NNX15AG76G to Penn State). ACT-America aircraft data can be found online (https://daac.ornl.gov/cgi-bin/dataset_lister.pl?p=37). We would like to thank J. Walega, P. Weibring, and D. Richter at NOAA INSTAAR for their work collecting ethane data. We thank C. Sweeney and B. Baier for flask sampling collection during the campaign, and P. Lang, E. Moglia, B. Miller, and M. Crotwell for analysis of the flask samples. We also thank J. Nowak at NASA Langley for his work with data collection. The authors declare no conflicts of interest with the submission of this manuscript.

References

Allen, D. T., Torres, V. M., Thomas, J., Sullivan, D. W., Harrison, M., Hendler, A., et al. (2013). Measurements of methane emissions at natural gas production sites in the United States. *National Academy of Sciences*, *110*(44), 17,768–17,773. https://doi.org/10.1073/pnas.1304880110

Alvarez, R. A., Zavala-Araiza, D., Lyon, D. R., Allen, D. T., Barkley, Z. R., Brandt, A. R., et al. (2018). Assessment of methane emissions from the U.S. oil and gas supply chain. *Science*. https://doi.org/10.1126/science.aar7204

Balashov, N. V., Davis, K. J., Miles, N. L., Lauvaux, T., Richardson, S. J., Barkley, Z. R., & Bonin, T. A. (2019). Background heterogeneity and other uncertainties in estimating urban methane flux: Results from the Indianapolis flux (influx) experiment. *Atmospheric Chemistry and Physics Discussions*, 1–39. https://doi.org/10.5194/acp-2019-48

Barkley, Z. R., Lauvaux, T., Davis, K. J., Deng, A., Fried, A., Weibring, P., et al. (2019). Estimating methane emissions from underground coal and natural gas production in southwestern Pennsylvania. *Geophysical Research Letters*, *46*(8), 4531–4540. https://doi.org/10.1029/2019GL082131

Barkley, Z. R., Lauvaux, T., Davis, K. J., Deng, A., Miles, N. L., Richardson, S. J., et al. (2017). Quantifying methane emissions from natural gas production in north-eastern Pennsylvania. *Atmospheric Chemistry and Physics*, *17*(22), 13,941–13,966. https://doi.org/10.5194/acp-17-13941-2017

Bloom, A. A., Bowman, K. W., Lee, M., Turner, A. J., Schroeder, R., Worden, J. R., et al. (2017). A global wetland methane emissions and uncertainty dataset for atmospheric chemical transport models (wetcharts version 1.0). *Geoscientific Model Development*, *10*(6), 2141–2156. https://doi.org/10.5194/gmd-10-2141-2017

Brandt, A. R., Heath, G. A., Kort, E. A., O'Sullivan, F., Pétron, G., Jordaan, S. M., et al. (2014). Methane leaks from North American natural gas systems. *Science*, *343*(6172), 733–735. https://doi.org/10.1126/science.1247045

Cardoso-Saldaña, F. J., Kimura, Y., Stanley, P., McGaughey, G., Herndon, S. C., Roscioli, J. R., et al. (2019). Use of light alkane fingerprints in attributing emissions from oil and gas production. *Environmental Science & Technology*, *53*(9), 5483–5492. https://doi.org/10.1021/acs.est.8b05828 pMID: 30912428

Cui, Y. Y., Brioude, J., Angevine, W. M., Peischl, J., McKeen, S. A., Kim, S.-W., et al. (2017). Top-down estimate of methane emissions in California using a mesoscale inverse modeling technique: The San Joaquin Valley. *Journal of Geophysical Research: Atmospheres*, *122*(6), 3686–3699. https://doi.org/10.1002/2016JD026398

Dee, D. P., Uppala, S. M., Simmons, A. J., Berrisford, P., Poli, P., Kobayashi, S., et al. (2011). The ERA-Interim reanalysis: Configuration and performance of the data assimilation system. *Quarterly Journal of the Royal Meteorological Society*, *137*(656), 553–597. https://doi.org/10.1002/qj.828

Desjardins, R., Worth, D., Pattey, E., VanderZaag, A., Srinivasan, R., Mauder, M., et al. (2018). The challenge of reconciling bottom-up agricultural methane emissions inventories with top-down measurements. *Agricultural and Forest Meteorology*, *248*, 48–59. https://doi.org/10.1016/j.agrformet.2017.09.003

Díaz-Isaac, L. I., Lauvaux, T., & Davis, K. J. (2018). Impact of physical parameterizations and initial conditions on simulated atmospheric transport and CO_2 mole fractions in the us midwest. *Atmospheric Chemistry and Physics*, *18*(20), 14,813–14,835. https://doi.org/10.5194/acp-18-14813-2018

DiGangi, J. P., Y. Choi, J. B. Nowak, H. Halliday, and M. M. Yang (2018). ACT-America: L2 in situ atmospheric CO_2, CO, CH_4, and O_3 concentrations, Eastern USA, doi:https://doi.org/10.3334/ORNLDAAC/1556,\ignorespacesoRNL\ignorespacesDAAC.

Dlugokencky, E. J., Myers, R. C., Lang, P. M., Masarie, K. A., Crotwell, A. M., Thoning, K. W., et al. (2005). Conversion of NOAA atmospheric dry air CH_4 mole fractions to a gravimetrically prepared standard scale. *Journal of Geophysical Research*, *110*(D18). https://doi.org/10.1029/2005JD006035

EDGAR (2011). Emissions database for global atmospheric research, available at http://edgar.jrc.ec.europa.eu/overview.php?v=42. .

Ellis, G. S. (2014). Geochemistry of natural gases of the anadarko basin, in Higley, D.K., compiler, Petroleum systems and assessment of undiscovered oil and gas in the Anadarko Basin Province, Colorado, Kansas, Oklahoma, and Texas—USGS Province 58: U.S. Geological Survey Digital Data Series DDS–69–EE, 31 p. Available at https://pubs.usgs.gov/dds/dds-069/dds-069-ee/pdf/dds69ee_Chapter4.pdf. .

Gherabati, S. A., Browning, J., Male, F., Ikonnikova, S. A., & McDaid, G. (2016). The impact of pressure and fluid property variation on well performance of liquid-rich eagle ford shale. *Journal of Natural Gas Science and Engineering*, *33*, 1056–1068. https://doi.org/10.1016/j.jngse.2016.06.019

Hristov, A. N., Harper, M., Meinen, R., Day, R., Lopes, J., Ott, T., et al. (2017). Discrepancies and uncertainties in bottom-up gridded inventories of livestock methane emissions for the contiguous united states. *Environmental Science & Technology*, *51*(23), 13,668–13,677. https://doi.org/10.1021/acs.est.7b03332 pMID: 29094590

Maasakkers, J. D., Jacob, D. J., Sulprizio, M. P., Turner, A. J., Weitz, M., Wirth, T., et al. (2016). Gridded national inventory of U.S. methane emissions. *Environmental Science & Technology*, *50*(23), 13,123–13,133. https://doi.org/10.1021/acs.est.6b02878 pMID: 27934278

McKain, K., Down, A., Raciti, S. M., Budney, J., Hutyra, L. R., Floerchinger, C., et al. (2015). Methane emissions from natural gas infrastructure and use in the urban region of Boston, Massachusetts. *Proceedings of the National Academy of Sciences*, *112*(7), 1941–1946. https://doi.org/10.1073/pnas.1416261112

Mesinger, F., DiMego, G., Kalnay, E., Mitchell, K., Shafran, P. C., Ebisuzaki, W., et al. (2006). North American regional reanalysis. *Bulletin of the American Meteorological Society*, *87*(3), 343–360. https://doi.org/10.1175/BAMS-87-3-343

Miller, S. M., Wofsy, S. C., Michalak, A. M., Kort, E. A., Andrews, A. E., Biraud, S. C., et al. (2013). Anthropogenic emissions of methane in the united states. *Proceedings of the National Academy of Sciences*, *110*(50), 20,018–20,022. https://doi.org/10.1073/pnas.1314392110

Mitchell, A. L., Tkacik, D. S., Roscioli, J. R., Herndon, S. C., Yacovitch, T. I., Martinez, D. M., et al. (2015). Measurements of methane emissions from natural gas gathering facilities and processing plants: Measurement results. *Environmental Science & Technology*, *49*(5), 3219–3227. https://doi.org/10.1021/es5052809 pMID: 25668106

Myhre, G., Shindell, D., Bréon, F.-M., Collins, W., Fuglestvedt, J., Huang, J., et al. (2013). Anthropogenic and Natural Radiative Forcing, *book section 8*. Cambridge, United Kingdom and New York, NY, USA: Cambridge University Press. https://doi.org/10.1017/CBO9781107415324.018

Omara, M., Zimmerman, N., Sullivan, M. R., Li, X., Ellis, A., Cesa, R., et al. (2018). Methane emissions from natural gas production sites in the united states: Data synthesis and national estimate. *Environmental Science & Technology*, *52*(21), 12,915–12,925. https://doi.org/10.1021/acs.est.8b03535 pMID: 30256618

Peischl, J., Eilerman, S. J., Neuman, J. A., Aikin, K. C., de Gouw, J., Gilman, J. B., et al. (2018). Quantifying methane and ethane emissions to the atmosphere from central and western u.s. oil and natural gas production regions. *Journal of Geophysical Research: Atmospheres*, *123*(14), 7725–7740. https://doi.org/10.1029/2018JD028622

Peischl, J., Karion, A., Sweeney, C., Kort, E. A., Smith, M. L., Brandt, A. R., et al. (2016). Quantifying atmospheric methane emissions from oil and natural gas production in the Bakken shale region of North Dakota. *Journal of Geophysical Research: Atmospheres*, *121*(10), 6101–6111. https://doi.org/10.1002/2015JD024631

Sheng, J.-X., Jacob, D. J., Maasakkers, J. D., Sulprizio, M. P., Zavala-Araiza, D., & Hamburg, S. P. (2017). A high-resolution (0.1° × 0.1°) inventory of methane emissions from Canadian and Mexican oil and gas systems. *Atmospheric Environment*, *158*, 211–215. https://doi.org/10.1016/j.atmosenv.2017.02.036

Sweeney, C., Karion, A., Wolter, S., Newberger, T., Guenther, D., Higgs, J. A., et al. (2015). Seasonal climatology of CO_2 across North America from aircraft measurements in the noaa/esrl global greenhouse gas reference network. *Journal of Geophysical Research: Atmospheres*, *120*(10), 5155–5190. https://doi.org/10.1002/2014JD022591

TCEQ (2012). Condensate tank oil and gas activities. Retrieved from https://www.tceq.texas.gov/assets/public/implementation/air/sip/hgb/RS_Report_Attachment_C.pdf

US Energy Information Administration (2018). U.S. dry natural gas production. Retrieved from https://www.eia.gov/dnav/ng/hist/n9070us2A.htm. Accessed October 2018.

US Environmental Protection Agency (2018). Inventory of U.S. greenhouse gas emissions and sinks: 1990–2016—Energy. Retrieved from https://www.epa.gov/sites/production/files/2018-01/documents/2018_chapter_3_energy.pdf. Accessed October 2018.

US Environmental Protection Agency (2019). Inventory of U.S. greenhouse gas emissions and sinks: 1990–2017. Retrieved from https://www.epa.gov/sites/production/files/2019-02/documents/us-ghg-inventory-2019-chapter-executive-summary.pdf. Accessed March 2019.

USDA (2014). 2012 census of agriculture. Retrieved from https://www.nass.usda.gov/Publications/AgCensus/2012/#full_report

Vaughn, T. L., Bell, C. S., Pickering, C. K., Schwietzke, S., Heath, G. A., Pétron, G., et al. (2018). Temporal variability largely explains top-down/bottom-up difference in methane emission estimates from a natural gas production region. *Proceedings of the National Academy of Sciences*, *115*(46), 11,712–11,717. https://doi.org/10.1073/pnas.1805687115

Zavala-Araiza, D., Lyon, D. R., Alvarez, R. A., Davis, K. J., Harriss, R., Herndon, S. C., et al. (2015). Reconciling divergent estimates of oil and gas methane emissions. *Proceedings of the National Academy of Sciences*, *112*(51), 15,597–15,602. https://doi.org/10.1073/pnas.1522126112

Zimmerle, D. J., Williams, L. L., Vaughn, T. L., Quinn, C., Subramanian, R., Duggan, G. P., et al. (2015). Methane emissions from the natural gas transmission and storage system in the United States. *Environmental Science & Technology*, *49*(15), 9374–9383. https://doi.org/10.1021/acs.est.5b01669 pMID: 26195284

Erratum

In the originally published version of this article, molecules were written with superscripts rather than subscripts. This error has since been corrected, and the present version may be considered the authoritative version of record.